Prism-coupled light emission from tunnel junctions containing interface roughness: Theory

A. Takeuchi, J. Watanabe, Y. Uehara, and S. Ushioda
Research Institute of Electrical Communication, Tohoku University, 2-1-1 Katahira, Sendai 980, Japan
(Received 25 April 1988)

We have developed a theory of prism-coupled light emission from tunnel junctions that incorporates the effect of roughness at all interfaces and have carried out a comprehensive numerical study of theoretical predictions. We assume a known current-fluctuation source due to tunneling electrons and calculate the radiated power using electromagnetic Green's functions for the multilayered tunnel-junction structure. The effect of roughness is incorporated in the Green's functions by a first-order perturbation method. We calculated the angle and energy dependence of *p*- and *s*-polarized emissions from both sides of a prototype tunnel junction that consists of a glass prism, an Al film, an Al oxide barrier, a Au film, and vacuum. The numerical results show that the *p*-polarized emission through the coupling prism occurs from the fast surface-plasmon mode, which is mainly generated by scattering of the slow surface-plasmon mode via interface roughness. The *p*-polarized emission from the vacuum side and the *s*-polarized emission from both sides arise from the direct conversion of the slow mode into external free photons via scattering by interface roughness. The emissions caused by roughness at different interfaces are calculated separately, and we conclude that the roughness at the oxide interfaces is most effective in causing light emission. This is because the slow mode which is most effectively excited by the tunneling current is localized at the oxide interfaces.

I. INTRODUCTION

By now it is well established that light emission from metal-oxide-metal tunnel junctions occurs via the excitation of surface plasmons by tunneling currents.[1] The tunnel-junction structure that consists of a glass substrate (or coupler prism), an Al film, Al oxide, and a counterelectrode (Au, Ag, etc.) supports three branches of surface plasmons, called the fast mode, the slow mode, and the intermediate mode (or prism-Al mode). Light emitted through the coupler prism originates from the fast mode which is radiative in the prism. Ushioda, Pierce, and Rutledge[2] (hereafter labeled paper I) experimentally demonstrated this emission mechanism, and also presented a theory to describe this process[3] (labeled paper II).

Earlier, Laks and Mills[4] (labeled paper III) gave a Green's-function treatment of light emission from a simplified junction structure consisting only of a semi-infinite Al, Al oxide, and a counterelectrode whose top surface has roughness. They assumed that the form of current fluctuations created by the tunneling current is given and proceeded to calculate the radiation from this source. The usually nonradiative surface plasmons at the counterelectrode-vacuum interface were made to radiate through scattering by surface roughness. Paper II was an extension of the Laks-Mills theory, and took account of the actual experimental junction structure which consists of five layers and four interfaces. Thus this theory reflects the true mode structure of the junction with three branches of surface plasmons, and could explain the kinematics of the emission process (emission-angle dependence). However, the treatment of paper II did not include surface roughness, and as a partial consequence, could not describe the emission spectra quantitatively. The observed emission spectra of paper I show a narrower peak than the prediction of the theory, and the peak position corresponds to the frequency region in which the slow mode is strongly excited. Thus it was surmised that residual surface roughness was converting the slow mode to the fast mode, and that the observed spectra reflected the density of states of the slow mode. Consequently, it was felt that a complete theory for a realistic junction structure that incorporates surface roughness is required to match the observed spectra.

The purpose of this paper is to present a theory of prism-coupled light emission from tunnel junctions with interface roughness. The present theory is capable of incorporating roughness at all four interfaces, including correlations among corrugations at different interfaces. The structure of the present theory is basically the same as that of paper III. We made their theory correspond more closely to the actual experimental geometry by extending it to the case of five layers and four interfaces. Also we have included interface roughness at all four interfaces rather than just at the top surface. To facilitate numerical computations of Green's functions for a multilayered structure, we make use of the 2×2 transfer matrix method that was used in another context.[5]

Some of the conclusions that we have reached from the numerical calculations are the ones anticipated in papers I and II. Indeed, the interface roughness induces conversion of the slow mode to the fast mode, and as a result the emission spectra reflect the high density of states of the slow mode and show a cutoff at about 2.2 eV (for Al–Al oxide–Au junction) where the dispersion curve of the slow mode approaches an asymptote. One new discovery we find interesting is that the dominant process for generation of the fast mode is not the direct channel by the

 ©1988 The American Physical Society

current but rather it is through conversion of the slow mode via interface roughness. Thus even though prism-coupled light emission occurs from the fast mode, the population distribution of the fast mode is mainly determined by the conversion of the slow mode.

In Sec. II we outline the structure of the theory and present analytical expressions for the emitted power with and without interface roughness. Section III contains the results of numerical computations and discussions of the results. In Sec. IV we consider the limitations of the present theory, and summarize the conclusions in Sec. V. Comparisons of the numerical results with experimental data are presented in a separate companion paper.[6]

II. THEORY

The real tunnel junctions are fabricated by first evaporating a thin film of Al on a glass substrate. Then the top of the Al film is oxidized to form an insulating barrier, and a counterelectrode is evaporated over the oxide layer. The metal and oxide layers have thicknesses on the order of 20 and 2 nm, respectively, and the glass substrate is very thick in comparison. Thus we model this structure by that shown in Fig. 1, where the top and bottom layers corresponding to glass and vacuum are semi-infinite along the z direction. The actual tunnel junction has only five layers, but here we develop a theory for a general n-layered structure having $n-1$ interfaces at $z=z_m$. The intermediate layers have thickness $d_m = z_m - z_{m-1}$, and dielectric constant ϵ_m which may be complex and may depend on frequency but spatially non-dispersive. We assume each interface to have roughness represented by a profile function $\zeta_m(\mathbf{x}_p)$, where $\mathbf{x}_p$ is a two-dimensional position vector in the average interface plane m.

The task of the theory is to find the electric field everywhere in this structure given a current distribution $\mathbf{J}(\mathbf{x},\omega)$, and eventually to calculate the power radiated into layers 1 and n. This is accomplished by following the Green's-function method used in paper III. Since the outline of the derivation is identical to the one given in paper III, we will not show the details of the necessary steps; we only exhibit crucial assumptions and results.

The electromagnetic Green's function $D_{\mu\nu}(\mathbf{x},\mathbf{x}';\omega)$ for the multilayered geometry is defined as a solution of the wave equation:

$$\sum_{\mu}\left[\frac{\omega^2}{c^2}\epsilon(\mathbf{x},\omega)\delta_{\lambda\mu}-\frac{\partial^2}{\partial x_\lambda \partial x_\mu}+\delta_{\lambda\mu}\nabla^2\right]D_{\mu\nu}(\mathbf{x},\mathbf{x}';\omega)=4\pi\delta_{\lambda\nu}\delta(\mathbf{x}-\mathbf{x}') , \tag{2.1}$$

where the frequency and position dependent dielectric constant $\epsilon(\mathbf{x},\omega)$ is given by

$$\epsilon(\mathbf{x},\omega)=\epsilon^{(0)}(z,\omega)+\Delta\epsilon(\mathbf{x},\omega) . \tag{2.2}$$

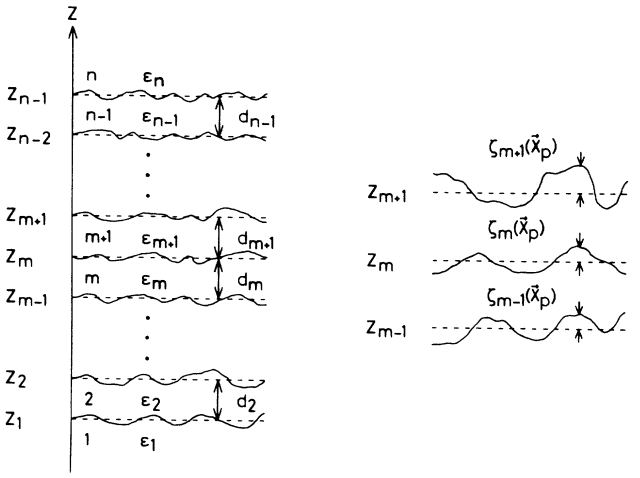

FIG. 1. The n-layered structure with $n-1$ rough interfaces at average plane $z=z_m$. The details of the interfaces are shown on the right with the definition of the interface profile functions $\zeta_m(\mathbf{x}_p)$.

Here $\epsilon^{(0)}(z,\omega)$ takes on appropriate values ϵ_m in respective layers between z_m and z_{m-1}. $\Delta\epsilon(\mathbf{x},\omega)$ is given by

$$\Delta\epsilon(\mathbf{x},\omega)=\begin{cases}\epsilon_m-\epsilon_{m+1} & \text{for } z_m<z<z_m+\zeta_m(\mathbf{x}_p)\\ 0 & \text{otherwise .}\end{cases} \tag{2.3}$$

We assume the current density $\mathbf{J}(\mathbf{x},t)$ to be a known quantity and write its μth component

$$J_\mu(\mathbf{x},t)=\int d\omega\frac{1}{2\pi}J_\mu(\mathbf{x};\omega)e^{-i\omega t} . \tag{2.4}$$

Then the μth component of the electric field at position $\mathbf{x}$ and frequency ω is given by

$$E_\mu(\mathbf{x},\omega)=-i\frac{\omega}{c^2}\sum_\nu\int d^3x' D_{\mu\nu}(\mathbf{x},\mathbf{x}';\omega)J_\nu(\mathbf{x}';\omega) \tag{2.5}$$

and the time-averaged power received per unit frequency per unit solid angle at position $\mathbf{x}$ far from the junction is

$$P(\mathbf{k}_p^{(0)},\omega)\equiv\frac{d^3W}{d\Omega\, d\omega\, dt}=|\mathbf{x}|^2\frac{\epsilon_n^{1/2}c}{8\pi}\sum_\mu\langle[E_\mu(\mathbf{x},\omega)]^*E_\mu(\mathbf{x},\omega)\rangle , \tag{2.6}$$

where $\langle\ \rangle$ means time average and $\mathbf{k}_p^{(0)}$ is the component of the wave vector of the emitted light parallel to the junction surface. In terms of the Green's functions, this power can be written

$$P(\mathbf{k}_p^{(0)},\omega)\equiv\frac{d^3W}{d\Omega\, d\omega\, dt}=\frac{\epsilon_n^{3/2}\omega^4\cos^2\theta_0}{32\pi^3c^5}\sum_\mu\sum_{\lambda,\lambda'}\int d^2Q_p\,dz'dz''[D_{\mu\lambda}(\mathbf{k}_p^{(0)},\mathbf{Q}_p,\omega\,|\,zz')]^*D_{\mu\lambda'}(\mathbf{k}_p^{(0)},\mathbf{Q}_p,\omega\,|\,zz'')\times J_{\lambda\lambda'}(\mathbf{Q}_p,\omega\,|\,z'z'') , \tag{2.7}$$

where $\mathbf{Q}_p$ is a two-dimensional wave vector in the plane of the junction. In Eq. (2.7) we have used the Fourier transform of the current-current correlation function $J_{\lambda\lambda'}(\mathbf{Q}_p,\omega \mid z'z'')$ defined by

$$\langle [J_\lambda(\mathbf{x}',\omega)]^* J_{\lambda'}(\mathbf{x}'',\omega)\rangle \equiv \int d^2Q_p e^{i\mathbf{Q}_p\cdot(\mathbf{x}_p''-\mathbf{x}_p')} J_{\lambda\lambda'}(\mathbf{Q}_p,\omega \mid z'z'') \quad (2.8)$$

and the two-dimensional Fourier transform of the Green's function defined by

$$D_{\mu\nu}(\mathbf{x},\mathbf{x}';\omega)=\int\int d^2k_p d^2k_p' \frac{1}{(2\pi)^4}\exp(i\mathbf{k}_p\cdot\mathbf{x}_p) \times\exp(-i\mathbf{k}_p'\cdot\mathbf{x}_p') D_{\mu\nu}(\mathbf{k}_p,\mathbf{k}_p',\omega \mid zz') . \quad (2.9)$$

The angle θ_0 is the angle of emission measured from the surface normal.

The Green's function $D_{\mu\nu}(\mathbf{x},\mathbf{x}';\omega)$ consists of two parts $D_{\mu\nu}^{(0)}$ and $D_{\mu\nu}^{(1)}$ and is written as

$$D_{\mu\nu}(\mathbf{x},\mathbf{x}';\omega)=D_{\mu\nu}^{(0)}(\mathbf{x},\mathbf{x}';\omega)+D_{\mu\nu}^{(1)}(\mathbf{x},\mathbf{x}';\omega) . \quad (2.10)$$

$D_{\mu\nu}^{(0)}$ is the solution of Eq. (2.1) for smooth interfaces; i.e., for $\zeta_m(\mathbf{x}_p)=0$ and $\Delta\epsilon(\mathbf{x},\omega)=0$ everywhere. $D_{\mu\nu}^{(1)}$ is the perturbation on $D_{\mu\nu}^{(0)}$ due to interface roughness and can be written in terms of $D_{\mu\nu}^{(0)}$ and the roughness profile $\zeta_m(\mathbf{x}_p)$ as

$$D_{\mu\nu}^{(0)}(\mathbf{x},\mathbf{x}';\omega)=\int d^2k_p \frac{1}{(2\pi)^2} e^{i\mathbf{k}_p\cdot(\mathbf{x}_p-\mathbf{x}_p')} d_{\mu\nu}^{(0)}(\mathbf{k}_p,\omega \mid zz') . \quad (2.12)$$

where z_{m+} (z_{m-}) means a position infinitesimally above (below) the interface at z_m. This equation was obtained by generalizing the perturbation method used in paper III.

It is convenient to use the two-dimensional Fourier transform of $D_{\mu\nu}^{(0)}(\mathbf{x},\mathbf{x}';\omega)$ for the smooth junction, and we define it by

$$D_{\mu\nu}^{(0)}(\mathbf{x},\mathbf{x}';\omega)=\int d^2k_p \frac{1}{(2\pi)^2} e^{i\mathbf{k}_p\cdot(\mathbf{x}_p-\mathbf{x}_p')} d_{\mu\nu}^{(0)}(\mathbf{k}_p,\omega \mid zz') . \quad (2.12)$$

Now we can write the power radiated in the absence of roughness $P^{(0)}$:

$$P^{(0)}(\mathbf{k}_p^{(0)},\omega)=\frac{A\epsilon_n^{3/2}\omega^4\cos^2\theta_0}{8\pi c^5}\sum_\mu\sum_{\lambda,\lambda'}\int\int dz\,dz''[d_{\mu\lambda}^{(0)}(\mathbf{k}_p^{(0)},\omega \mid zz')]^* d_{\mu\lambda'}^{(0)}(\mathbf{k}_p^{(0)},\omega \mid zz'') J_{\lambda\lambda'}(\mathbf{k}_p^{(0)},\omega \mid z'z'') \quad (2.13)$$

and the roughness mediated emission:

$$P^{(1)}(\mathbf{k}_p^{(0)},\omega)=\frac{\epsilon_n^{3/2}\omega^8\cos^2\theta_0}{512\pi^5c^9}\sum_\mu\sum_{\lambda,\lambda'}\sum_{\eta,\eta'}\sum_{m,m'}\int d^2Q_p\,dz'dz''[(\epsilon_m-\epsilon_{m+1})]^*(\epsilon_{m'}-\epsilon_{m'+1})[d_{\mu\eta}^{(0)}(\mathbf{k}_p^{(0)},\omega \mid z,z_{m+})]^* \times d_{\mu\eta'}^{(0)}(\mathbf{k}_p^{(0)},\omega \mid z,z_{m'+})[\zeta_m(\mathbf{k}_p^{(0)}-\mathbf{Q}_p)]^*\zeta_{m'}(\mathbf{k}_p^{(0)}-\mathbf{Q}_p) \times[d_{\eta\lambda}^{(0)}(\mathbf{Q}_p,\omega \mid z_{m-},z')]^* d_{\eta'\lambda'}^{(0)}(\mathbf{Q}_p,\omega \mid z_{m'-},z'')J_{\lambda\lambda'}(\mathbf{Q}_p,\omega \mid z'z'') , \quad (2.14)$$

where $\zeta_m(\mathbf{k}_p^{(0)}-\mathbf{Q}_p)$ is the two-dimensional Fourier transform of $\zeta_m(\mathbf{x}_p)$.

We can interpret the meaning of Eqs. (2.13) and (2.14) as follows. In the absence of interface roughness Eq. (2.13), the current fluctuation $J_{\lambda\lambda'}(\mathbf{k}_p^{(0)},\omega \mid z'z'')$ at $\mathbf{k}_p=\mathbf{k}_p^{(0)}$ excites surface plasmons at the same wave vector $\mathbf{k}_p^{(0)}$, and the surface plasmons in turn radiate light with the same value of the wave vector parallel to the interface. On the other hand, when there is interface roughness present, the current fluctuation $J_{\lambda\lambda'}(\mathbf{Q}_p,\omega \mid z'z'')$ with the wave vector $\mathbf{Q}_p$ excites surface plasmons whose wave vector is also $\mathbf{Q}_p$. Then these surface plasmons are scattered by interface roughness $\zeta_m(\mathbf{k}_p^{(0)}-\mathbf{Q}_p)$ into surface plasmons with the wave vector $\mathbf{k}_p^{(0)}$. To sum over all possible surface plasmons that scatter into the mode with wave vector $\mathbf{k}_p^{(0)}$, we integrate over $\mathbf{Q}_p$ in the plane. Also the scattering contributions from different interfaces are counted by the sum over indices m and m'. Thus the total radiated power is given by

$$P(\mathbf{k}_p^{(0)},\omega)=P^{(0)}(\mathbf{k}_p^{(0)},\omega)+P^{(1)}(\mathbf{k}_p^{(0)},\omega) . \quad (2.15)$$

Next we write $d_{\mu\nu}^{(0)}(\mathbf{k}_p,\omega \mid z'z'')$ in terms of two linearly independent solutions of the homogeneous wave equation corresponding to Eq. (2.1), $E_\mu^<(k_p,z)$ and $E_\mu^>(k_p,z)$. These are the solutions that remain finite either for $z\to\infty$ or for $z\to-\infty$, and in each layer m can be written in the form

$$E_\mu^{>,<}(k_p,z)=\{A_\mu^{>,<}\exp[ik_z(m)(z-z_{m-1})] +B_\mu^{>,<}\exp[-ik_z(m)(z-z_{m-1})]\} \times\exp[i(k_px-\omega t)] , \quad (2.16)$$

where

$$k_z(m)=\left[\frac{\epsilon_m\omega^2}{c^2}-k_p^2\right]^{1/2}. \tag{2.17}$$

In taking the square root in Eq. (2.17), we choose the root so that $\mathrm{Im}k_z(m)\geq 0$. $A_\mu^{>,<}$ and $B_\mu^{>,<}$ are the amplitudes for the upward and downward propagating waves, respectively. These amplitudes are determined by the 2×2 transfer matrix method described by Kurosawa, Pierce, and Ushioda.[5] In order to satisfy the boundary conditions at $z\rightarrow\pm\infty$, we set

$$A_\mu^{>}(k_p,n)=1, B_\mu^{>}(k_p,n)=0 \tag{2.18}$$

and

$$A_\mu^{<}(k_p,1)=0, B_\mu^{<}(k_p,1)=1 \tag{2.19}$$

and determine the rest of the amplitudes using the 2×2 transfer matrices for the present structure.

At this point we introduce a simplifying assumption that was also used in paper III; i.e., we assume that the only nonzero component of the current-current correlation function is

$$J_{zz}(Q_p,\omega|z'z'')=\frac{eI_0(1-\hbar\omega/eV_0)}{2\pi^2 A}\frac{\Delta(z',z'')}{(1+Q_p^2\xi_0^2)^{3/2}} \tag{2.20}$$

and further that $\Delta(z',z'')=1$ only in the oxide layer and zero otherwise. In Eq. (2.20), e is the electron charge; I_0 and V_0 are the dc tunneling current and the bias voltage across the junction, respectively; A is the junction area, and ξ_0 is the spatial correlation distance in the current fluctuation.

Another assumption we require in order to proceed to numerical computation is that the interface roughness has a Gaussian distribution in the sense that

$$|\zeta_m(\mathbf{k}_p^{(0)}-\mathbf{Q}_p)|^2=\pi A a^2\delta^2\exp(-\tfrac{1}{4}a^2|\mathbf{k}_p^{(0)}-\mathbf{Q}_p|^2), \tag{2.21}$$

where a is the correlation distance between peaks of the roughness, and δ is the root-mean-square amplitude of the roughness.

Now we can write radiated power in terms of the electric field amplitudes defined above:

$$P^{(0)}(k_p^{(0)},\omega)=\frac{\pi A\epsilon^{1/2}\omega^2\sin^2\theta_0}{2c^3|B_z^{<}(k_p^{(0)},n)|^2}\int\int dz'dz''[E_z^{<}(k_p^{(0)},z')]^*E_z^{<}(k_p^{(0)},z'')J_{zz}(k_p^{(0)},\omega|z'z''), \tag{2.22}$$

where $B_\mu^{<}(k_p^{(0)},n)$ is the amplitude defined in Eq. (2.16) evaluated in layer n at $k_p=k_p^{(0)}$, and

$$P^{(1)}(k_p^{(0)},\omega)=\frac{\omega^2}{32\pi c^3\epsilon_n^{3/2}}\sum_{mm'}[(\epsilon_m-\epsilon_{m+1})]^*(\epsilon_{m'}-\epsilon_{m'+1})$$

$$\begin{aligned}
&\times\int\int\int\int d\phi\, dQ_p dz'dz''\frac{Q_p^5}{|k_z(Q_p,n)|^2|B_z^{<}(Q_p,n)|^2}[\zeta_m(\mathbf{k}_p^{(0)}-\mathbf{Q}_p)]^*\zeta_{m'}(\mathbf{k}_p^{(0)}-\mathbf{Q}_p)\\
&\times(\Theta(z_{m-}-z')\Theta(z_{m'-}-z'')[E_z^{<}(Q_p,z')]^*E_z^{<}(Q_p,z'')J_{zz}(Q_p,\omega|z'z'')\\
&\quad\times\{(E_{xx}+E_{yy})[E_x^{>}(Q_p,z_{m-})]^*E_x^{>}(Q_p,z_{m'-})+E_{xz}[E_x^{>}(Q_p,z_{m-})]^*E_z^{>}(Q_p,z_{m'-})\\
&\qquad+E_{zx}[E_z^{>}(Q_p,z_{m-})]^*E_x^{>}(Q_p,z_{m'-})+E_{zz}[E_z^{>}(Q_p,z_{m-})]^*E_z^{>}(Q_p,z_{m'-})\}\\
&+\Theta(z_{m-}-z')\Theta(z''-z_{m'-})[E_z^{<}(Q_p,z')]^*E_z^{>}(Q_p,z'')J_{zz}(Q_p,\omega|z'z'')\\
&\times\{(E_{xx}+E_{yy})[E_x^{>}(Q_p,z_{m-})]^*E_x^{<}(Q_p,z_{m'-})+E_{xz}[E_x^{>}(Q_p,z_{m-})]^*E_z^{<}(Q_p,z_{m'-})\\
&\quad+E_{zx}[E_z^{>}(Q_p,z_{m-})]^*E_x^{<}(Q_p,z_{m'-})+E_{zz}[E_z^{>}(Q_p,z_{m-})]^*E_z^{<}(Q_p,z_{m'-})\}\\
&+\Theta(z'-z_{m'-})\Theta(z_{m'-}-z'')[E_z^{>}(Q_p,z')]^*E_z^{<}(Q_p,z'')J_{zz}(Q_p,\omega|z'z'')\\
&\times\{(E_{xx}+E_{yy})[E_x^{<}(Q_p,z_{m-})]^*E_x^{>}(Q_p,z_{m'-})\\
&\quad+E_{xz}[E_x^{<}(Q_p,z_{m-})]^*E_z^{>}(Q_p,z_{m'-})+E_{zx}[E_z^{<}(Q_p,z_{m-})]^*E_x^{>}(Q_p,z_{m'-})\\
&\quad+E_{zz}[E_z^{<}(Q_p,z_{m-})]^*E_z^{>}(Q_p,z_{m'-})\}\\
&+\Theta(z'-z_{m-})\Theta(z''-z_{m'-})[E_z^{>}(Q_p,z')]^*E_z^{>}(Q_p,z'')J_{zz}(Q_p,\omega|z'z'')\\
&\times\{(E_{xx}+E_{yy})[E_x^{<}(Q_p,z_{m-})]^*E_x^{<}(Q_p,z_{m'-})+E_{xz}[E_x^{<}(Q_p,z_{m-})]^*E_x^{<}(Q_p,z_{m'-})\\
&\quad+E_{zx}[E_z^{<}(Q_p,z_{m-})]^*E_x^{<}(Q_p,z_{m'-})+E_{zz}[E_z^{<}(Q_p,z_{m-})]^*E_z^{<}(Q_p,z_{m'-})\}).
\end{aligned} \tag{2.23}$$

We have introduced new symbols $E_{\mu\nu}$ in order to simplify the notation. They are defined by the following equations:

$$E_{xx} \equiv \frac{1}{|B_z^<(k_p^{(0)},n)|^2}(\sin^2\theta_0)(\cos^2\phi_0)[E_x^<(k_p^{(0)},z_{m+})]^* \times E_x^<(k_p^{(0)},z_{m'+}) , \quad (2.24)$$

$$E_{yy} \equiv \frac{1}{|B_y^<(k_p^{(0)},n)|^2}(\sin^2\phi_0)[E_y^<(k_p^{(0)},z_{m+})]^* \times E_y^<(k_p^{(0)},z_{m'+}) , \quad (2.25)$$

$$E_{xz} \equiv \frac{1}{|B_z^<(k_p^{(0)},n)|^2}(\sin^2\theta_0)(\cos\phi_0)[E_x^<(k_p^{(0)},z_{m+})]^* \times E_z^<(k_p^{(0)},z_{m'+}) , \quad (2.26)$$

$$E_{zx} \equiv \frac{1}{|B_z^<(k_p^{(0)},n)|^2}(\sin^2\theta_0)(\cos\phi_0)[E_z^<(k_p^{(0)},z_{m+})]^* \times E_x^<(k_p^{(0)},z_{m'+}) , \quad (2.27)$$

$$E_{zz} \equiv \frac{1}{|B_z^<(k_p^{(0)},n)|^2}(\sin^2\theta_0)[E_z^<(k_p^{(0)},z_{m+})]^* \times E_z^<(k_p^{(0)},z_{m'+}) , \quad (2.28)$$

where ϕ_0 is the azimuthal angle of emission measured from the direction of the x axis.

Equations (2.22) and (2.23) are the main results that we will use in numerical computations in the following section.

III. NUMERICAL STUDY

In this section we present the results of numerical computations of the angle and energy dependence of light emission from tunnel junctions obtained by Eqs. (2.22) and (2.23). Numerical calculations have been carried out using a high speed computer for a prototypical tunnel-junction structure that consists of five layers, glass (prism), Al (20 nm), oxide (3 nm), Au (20 nm), and vacuum. The surface roughness parameters we assume for the prototype junction throughout this calculation are $a=20$ nm and $\delta=3.5$ nm, unless otherwise specified. We assumed that there is no correlation between corrugated profiles $\zeta_m(\mathbf{x}_p)$ and $\zeta_{m'}(\mathbf{x}_p)$ at different interfaces. The special correlation distance for the current fluctuation ξ_0 was set equal to 10 nm for all calculations. The angle dependence of emission presented in this paper was calculated for a fixed frequency at $\lambda=600$ nm (2.07 eV) for all cases.

The dielectric constant of the borosilicate crown glass (BK-7 prism) was calculated at each frequency from the dispersion formula for this glass. For the oxide layer we used the value for sapphire ($\epsilon=3.1$). The dielectric constant for Al was obtained by interpolation from the data compiled by Ordal *et al.*,[7] and for Au it was found from the data given by Johnson and Christy.[8]

Figure 2 shows the dispersion curves for surface plasmons for the smooth junction. These curves were found by following the peaks of $1/|B_z^<(k_p,5)|^2$ in the (k_p,ω) plane for real k_p and ω. This method was used because it is difficult to find the complex roots of $B_z^<(k_p,\omega)=0$.

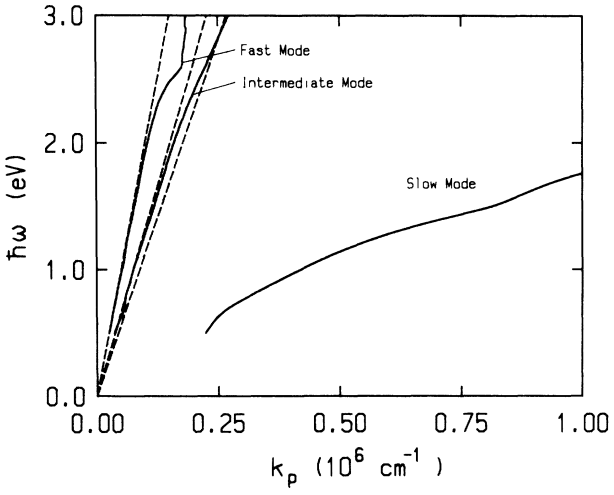

FIG. 2. Dispersion curves of the three branches of surface-plasmon modes for the smooth prototype junction structure consisting of BK-7 glass, Al (20 nm), Al oxide (3 nm), Au (20 nm), and vacuum. The three dashed lines are the light lines in vacuum, prism, and oxide from the left, respectively. The structures on the curves arise from the structures in the dielectric functions.

The dispersion curves for the fast mode and the prism-Al mode are asymptotic to the vacuum light line and the prism light line, respectively, for small values of k_p, and both curves rise smoothly through the visible frequency region. The slow mode has the upper cutoff around 2.2 eV for which the wave vector parallel to the interface becomes very large.

Figure 3 illustrates three-dimensional plots of $P^{(0)}(k_p,\omega)$ over the (k_p,ω) plane for $V_0=3.0$ V. The vertical axis is proportional to $P^{(0)}(k_p,\omega)$. Figure 3(a) uses a large vertical scale to show the overall structure, and Fig. 3(b) shows the details near the vacuum light line. The dominant feature is the peak due to the slow mode whose dispersion curve has an asymptote around 2.2 eV. Since this mode lies to the right side of the prism light line, it is nonradiative, but we see that it is most strongly excited by tunneling currents. These figures are most useful in visualizing the mode structure and the strengths of excitation of each mode.

In the following we study the angle, polarization, and energy dependence of light emission from the prism side and the vacuum side for the junction as specified above.

A. Emission angle dependence

Figures 4–6 depict the angle dependence of the emission intensity from the prism side. In Fig. 4 we show the angle dependence of emission at $\lambda=600$ nm for a junction without interface roughness. The intensity is normalized to unity at the peak, and we use the same normalization constant for the intensity for all the angle

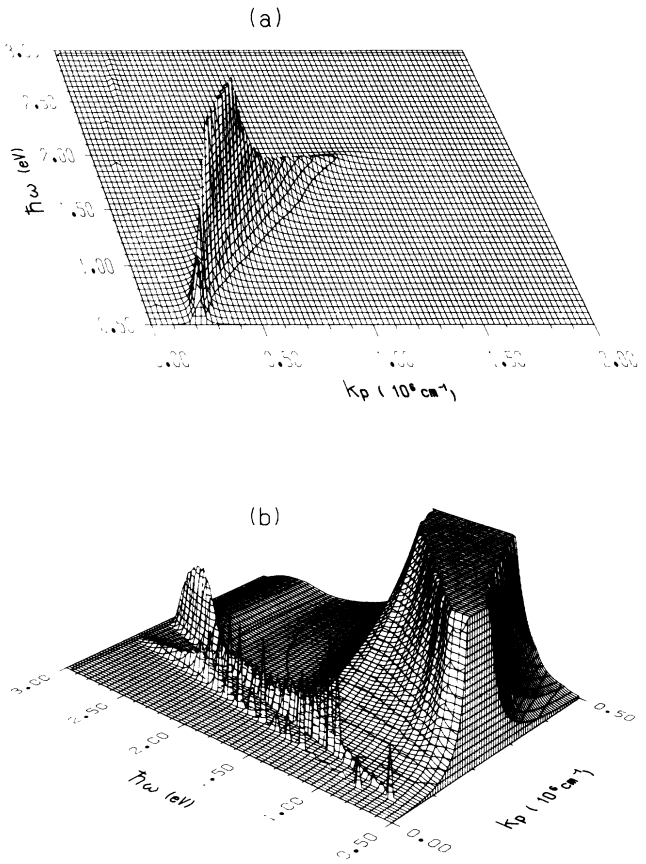

FIG. 3. (a) Large scale contour plot of the power density of surface-plasmon modes on the (k_p,ω) plane. The large peak is due to the slow mode. (b) Enlarged view of the same plot near the light line showing the peaks due to the intermediate (prism-Al) modes and the fast modes.

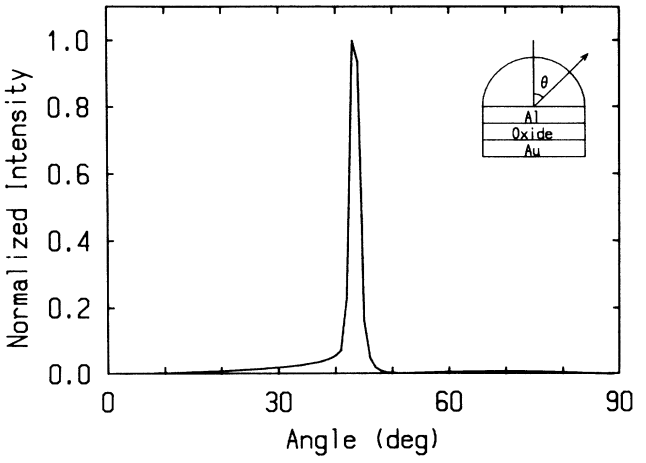

FIG. 4. Angle dependence of p-polarized emission through the prism at $\lambda=600$ nm for the smooth prototype junction. The intensity scale is normalized to unity at the peak. The same normalization is used in all figures through Fig. 9.

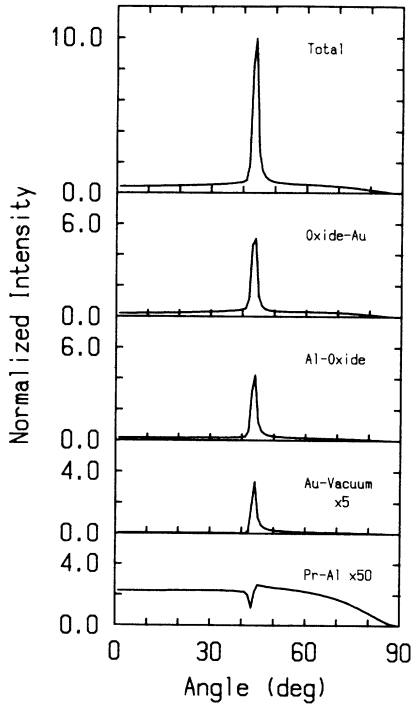

FIG. 5. Angle dependence of p-polarized emission on the prism side for the roughened prototype junction at $\lambda=600$ nm. The roughness parameters are $a=20$ nm and $\delta=3.5$ nm. The contributions from different rough interfaces are shown separately.

dependence plots that follow. Thus relative strengths of emission for different conditions may be compared. The sharp peak at 43° is due to the radiative fast mode whose wave vector parallel to the interface matches that of the light in the prism. Thus this peak appears even for a smooth junction. This is the emission peak discussed in paper II for smooth junctions. There is only p-polarized emission and no emission with s polarization.

Figure 5 shows the angle dependence of p-polarized

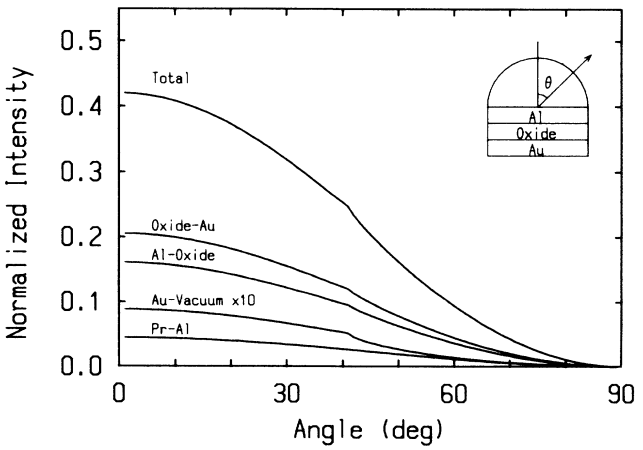

FIG. 6. Angle dependence of s-polarized emission through the prism for the roughened prototype junction.

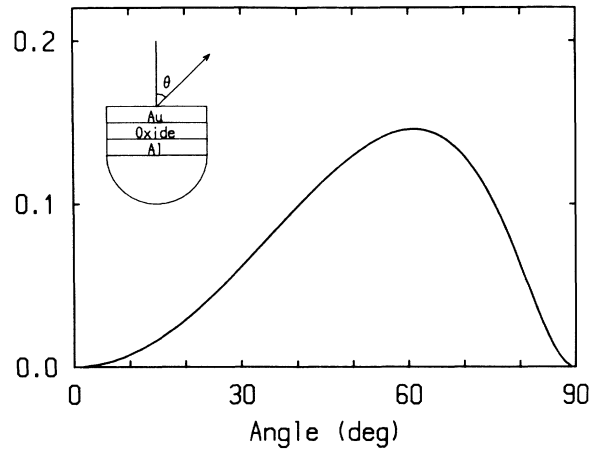

FIG. 7. Angle dependence of p-polarized emission on the Au-vacuum side for the smooth prototype junction.

emission intensity for a roughened junction also at $\lambda=600$ nm. The roughness parameters are $a=20$ nm and $\delta=3.5$ nm, and the same roughness is assumed at all interfaces. The contributions from roughness at different interfaces are shown separately. We see that the roughness of the oxide metal interfaces is the most effective in inducing emission. This is understandable in view of the fact that the slow mode which is most strongly excited is localized across the oxide layer. Thus the slow mode is most effectively scattered by the roughness of the oxide interfaces.

The second important feature that we note in Fig. 5 is the presence of the strong peak at 43° which coincides with the location of the peak for the smooth junction of Fig. 4. The presence of this peak shows that most of the light is emitted by the fast mode as in the case of the smooth junction. We also note that there is a low but finite background of emission intensities at all angles, and that the background contribution from the roughness at the prism-Al interface has a dip near 43° instead of a peak. (This dip is apparently caused by resonant excitation of the fast mode through interface roughness. This

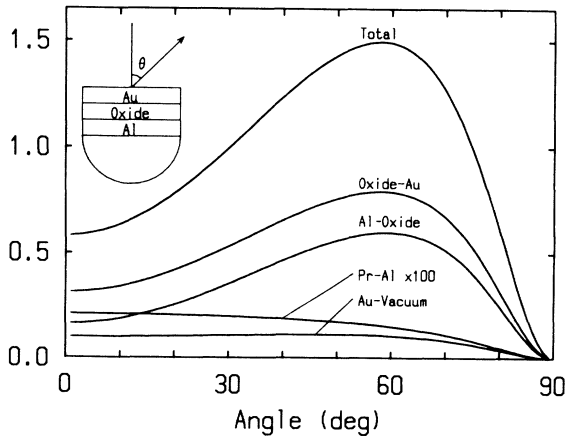

FIG. 8. Angle dependence of p-polarized emission on the Au-vacuum side for the roughened prototype junction. The contributions from different interfaces are shown separately.

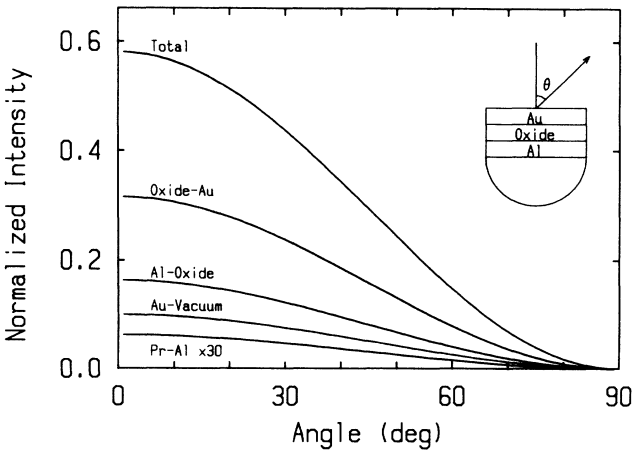

FIG. 9. Angle dependence of s-polarized emission on the Au-vacuum side for the roughened prototype junction. The contributions from different interfaces are shown separately.

process counts as a loss in the direct conversion of the slow mode to external photons which this plot represents.) The relative intensities at the peak and for the background can be fitted by adjusting the mean-square roughness δ. This can be a useful way of estimating δ when we compare theory with experimental data.

A comparison with Fig. 4 shows that emission due to roughness (for $\delta=3.5$ nm) is about 10 times stronger than that from the smooth junction. Since the contribution from roughness is proportional to δ^2, this ratio can be adjusted to fit experimental data.

For a roughened junction s-polarized emission is also allowed, and the angle dependence is shown in Fig. 6. The overall intensity is much lower than the p-polarized emission, and the strongest emission occurs normal to the junction. In this case again the roughness at the oxide in-

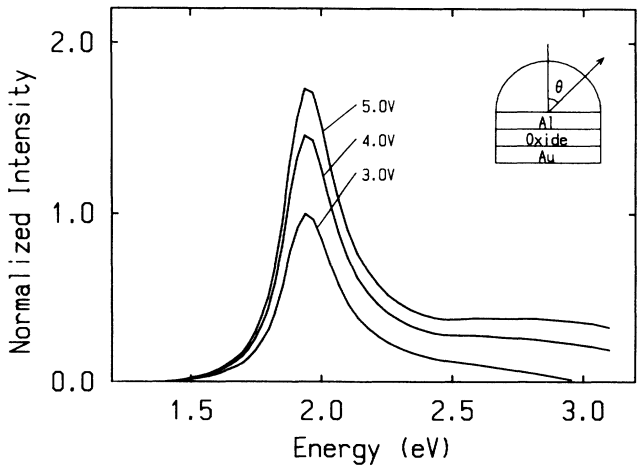

FIG. 10. p-polarized emission spectrum through the prism for the smooth prototype junction for different bias voltages. The intensity scale is normalized at the peak of the curve for the bias voltage of 3.0 V. The same normalization is used for all figures through Fig. 19.

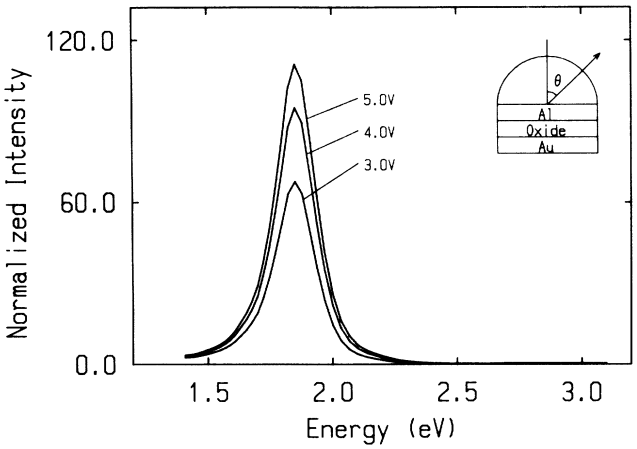

FIG. 11. p-polarized emission spectrum through the prism for the roughened prototype junction for different bias voltages.

terfaces contributes most and the roughness at the Au-vacuum interface is the least effective. We note a small bend at 43°, but otherwise there is no strong feature. This radiation pattern is analogous to that from a dipole lying in the plane of the junction.

Next we consider the angle dependence of emission from the Au side into vacuum which is shown in Figs. 7–9. The so-called "direct emission" shown in Fig. 7 for the smooth junction is p polarized. It is an order of magnitude weaker than on the prism side. (There is no s-polarized direct emission.) This emission arises directly from the current fluctuations and not through the excitation of surface plasmons. It has the feature of dipole emission from a dipole lying normal to the layers. This is a natural result, since we assumed that all components of $J_{\lambda\lambda'}(\mathbf{k}_p^{(0)},\omega \mid z'z'')$ except for $J_{zz}(\mathbf{k}_p^{(0)},\omega \mid z'z'')$ are zero.

The roughness-induced emissions for p and s polarizations are illustrated in Figs. 8 and 9, respectively. Here again the roughness at the oxide interfaces are the most effective and at the prism-Al interface the least effective. The overall angle dependence for p-polarized light is

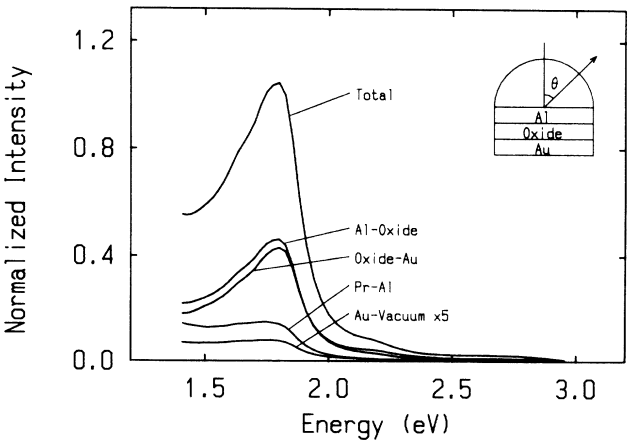

FIG. 12. s-polarized emission spectrum through the prism for the roughened prototype junction. The contributions from different interfaces are shown separately.

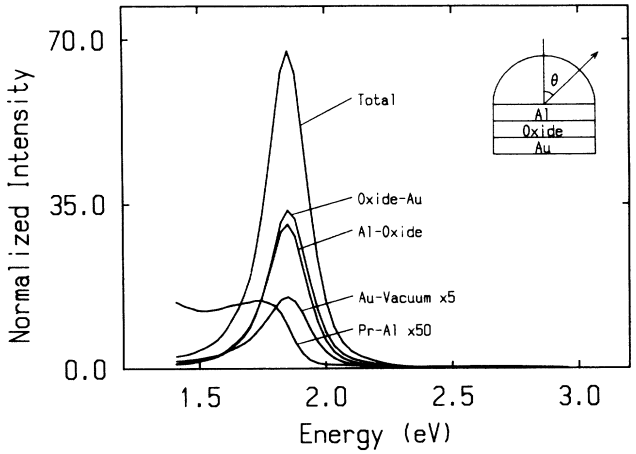

FIG. 13. p-polarized emission spectrum through the prism for the roughened prototype junction, showing separate contributions from different interfaces. The roughness parameters are those of the prototype: $a=20$ nm, $\delta=3.5$ nm. (Same junction as in Fig. 11 for the bias voltage of 3.0 V.)

similar to the emission pattern from a dipole lying normal to the layers. The s-polarized emission pattern is analogous to that of a dipole lying in the plane of the layers.

From the fact that most of the light emission is caused by the roughness at the oxide interfaces (where the slow mode is localized) and that the angle dependence shows the dipole pattern, we may conclude that the emission into the vacuum side mostly results from the direct conversion of the slow mode into external light (free photons) by interface roughness.

B. Energy dependence

Now let us consider the emission spectra (energy dependence) for a fixed angle of emission. All the spectra we present here are for emission at 43°. First we consider emission on the prism side. Figure 10 shows the emission spectra for different bias voltages V_0 across the junction for a smooth junction. The peak of emission is located about 1.9 eV and the spectra extend to the upper cutoff at eV_0. The intensity scale is normalized to unity at the peak of the spectrum for the bias voltage of 3.0 V. This normalization scale is used for all the spectra that follow. Thus relative intensities for different junctions may be compared directly by looking at the calibrations on the vertical scale. Figure 10 is for p-polarized emission, and there is no s-polarized emission from a smooth junction.

We show the corresponding p-polarized spectra for a junction with the standard roughness parameters ($\delta=3.5$ nm and $a=20$ nm) in Fig. 11. Note that the intensity scale is about 60 times that of Fig. 10, indicating much stronger emission from the roughened junction. We also note that the upper cutoff is around 2.2 eV regardless of the bias voltage. This upper cutoff energy matches the asymptotic energy of the slow mode dispersion curve. This is another piece of evidence that indicates that emission is dominated by the fast mode created by conversion of the slow mode through scattering by interface rough-

ness.

Figure 12 depicts the s-polarized spectrum showing separate contributions from the roughness at different interfaces. The bias voltage is 3.0 V. This spectrum also diminishes beyond 2.2 eV, but the cutoff is less sharp than the case of p-polarized spectra.

Figures 13–15 are presented to indicate the change in emission spectra for different values of the correlation distance a of interface roughness. The root-mean-square roughness amplitude δ is fixed at 3.5 nm, and the bias voltage is 3.0 V for all three spectra. The parameters for Fig. 13 are the same as for Fig. 11, but we now show separate contributions from different interfaces. We see that the overall intensity is highest for $a=20$ nm and $\frac{1}{10}$ and $\frac{1}{5}$ for $a=50$ nm and $a=5$ nm, respectively. This dependence on the roughness correlation distance a has a clear physical interpretation. The amount of wave-vector transfer that takes place upon single scattering by roughness is on the order of $2/a$. [See Eq. (2.20).] Since the distance between the dispersion curves for the slow mode and the fast mode is on the order of 1×10^6 cm^{-1} (see Figs. 2 and 3) around 1.8–1.9 eV, the value of a about 20 nm is most effective in converting the slow mode into the fast mode at these energies. When $a=5$ nm, the most efficient wave-vector transfer occurs around 4×10^6 cm^{-1}. Thus we see this contribution above 2 eV in Fig. 15. On the other hand for $a=50$ nm, the most effective wave-vector transfer occurs for 4×10^5 cm^{-1}. This contribution appears on the low-energy side below 1.5 eV as seen in Fig. 14.

Now let us look at the emission spectra from the Au-vacuum side. Figure 16 shows the direct emission for a smooth junction with the bias voltage of 3.0 V. (All the spectra that follow have the same bias voltage.) Note that the intensity scale is about $\frac{1}{20}$ of the direct emission from the prism side. The spectrum has a broad peak centered between 2.0 and 2.5 eV.

To check our results with that of paper III, we made the Al layer infinitely thick by taking the prism away, and obtained the spectrum in Fig. 17. This spectrum agrees with the corresponding spectrum presented in paper III. By comparing with Fig. 10, we see that the emission on the Au-vacuum side is comparable to that on the prism side when it is present.

Figures 18 and 19 illustrate the p- and s-polarized emission spectra due to interface roughness on the Au-vacuum side. Again the roughness at the oxide interfaces contributes most strongly to the emission as the decomposition of different contributions shows. The spectral shapes for p and s polarizations are essentially identical having a well-defined peak at about 1.8 eV, but the intensities are different by about a factor of 6. By comparing the spectra in Figs. 11, 12, 18, and 19, we see that the s-polarized emission on both sides and the p-polarized emission on the Au-vacuum side are all quite similar in shape. The p-polarized emission through the prism shown in Fig. 11 is the unique one among the four. From the sharp peak in the angle dependence shown in Fig. 5, we know that this emission arises from the fast mode, regardless of how it is generated. On the other hand the s-polarized emission from both sides and the p-polarized

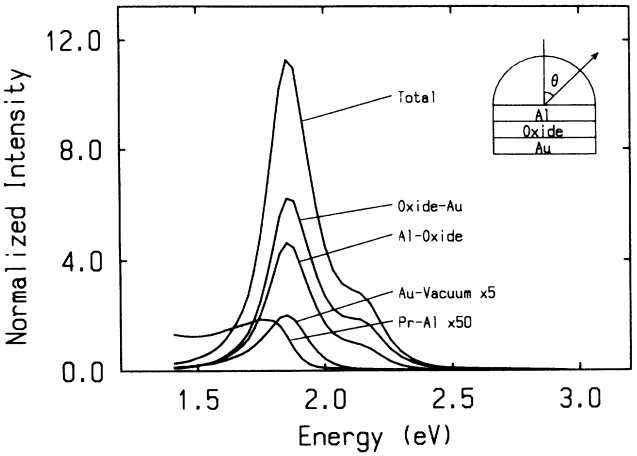

FIG. 15. All parameters are the same as in Fig. 13, except for the value of $a=5$ nm.

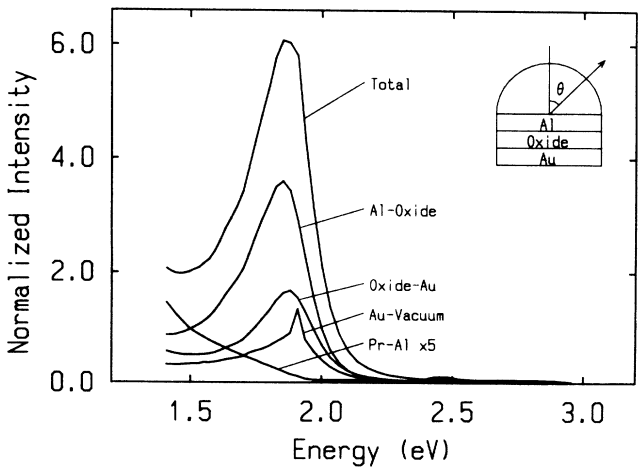

FIG. 14. All parameters are the same as in Fig. 13, except for the correlation distance of roughness, $a=50$ nm.

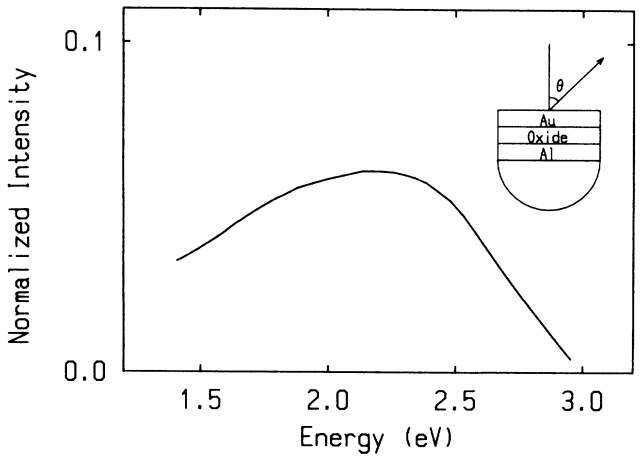

FIG. 16. p-polarized emission spectrum from the Au-vacuum side for the smooth prototype junction (direct emission).

emission from the Au-vacuum side (Figs. 6, 8, and 9) have the angle dependence characteristic of radiation from a dipole lying either perpendicular or parallel to the junction plane.

From these pieces of evidence we can arrive at the following conclusion. The roughness-induced emission from the prism side (Figs. 5 and 11) arises from the conversion of the slow mode to the fast mode and subsequent emission by the fast mode. On the other hand all the emission on the Au-vacuum side and the *s*-polarized emission from the prism side are caused by direct conversion of the slow mode to external light via scattering by interface roughness.

IV. DISCUSSION

As we have seen in the previous comprehensive numerical study, the present theory produces results that are consistent with the physical picture of the emission processes of the light-emitting tunnel junction with interface roughness. By carrying out numerical calculations for varied parameters and emission geometries, we have not only confirmed what was anticipated on physical grounds before but also gained new insight into the light emission process, particularly on the role played by interface roughness. The main improvement over the theory of papers II and III is the inclusion of roughness at arbitrary interfaces and inclusion of the coupling prism. Also the use of the 2×2 transfer matrix method made it possible to carry out numerical computations without going through complicated algebra analytically.

The present work brings the theory one step closer to experimental reality. However, one must remember that the theoretical framework set by paper III has its limits. The most important assumption contained in the present theory is the form of the current fluctuations given by $J_{\lambda\lambda'}(\mathbf{k}_p^{(0)},\omega \mid z'z'')$. This form is derived by using several simplifying assumptions about the nature of the tunneling current (see paper III), and one should not hold too much faith in this form of the current fluctuation. Furthermore, we have assumed that $J_{\lambda\lambda'}(\mathbf{k}_p^{(0)},\omega \mid z'z'')=0$ for components other than $J_{zz}(\mathbf{k}_p^{(0)},\omega \mid z'z'')$, and that even this component is zero outside the oxide layer. These assumptions need be examined more closely as we start comparing the details of emission spectra and angle dependence with experiment.

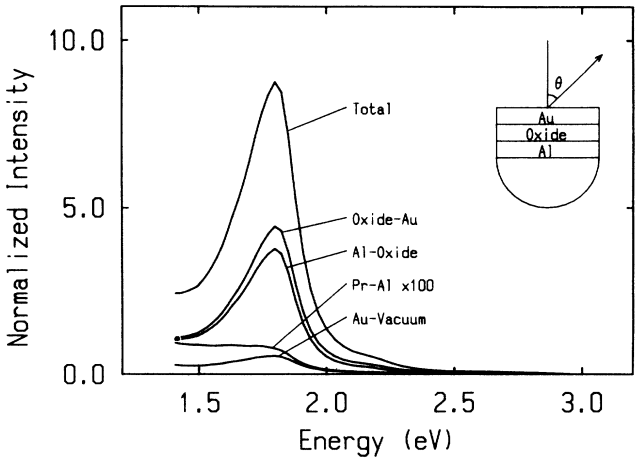

FIG. 18. *p*-polarized emission spectrum on the Au-vacuum side for the roughened prototype junction. The contributions from different interfaces are shown separately.

The Green's functions for smooth interfaces are exact, and there is no uncertain factor for emission from the smooth junction, once $J_{\lambda\lambda'}(\mathbf{k}_p^{(0)},\omega|z'z'')$ is known. Thus, it was hoped[2] earlier that measurement of the *p*-polarized emission from the prism side will allow precise determination of the form of current fluctuations. However, the present study shows that even the prism coupled emission is dominated by emission caused by a small amount of roughness. Thus it is not feasible to determine $J_{\lambda\lambda'}(\mathbf{k}_p^{(0)},\omega|z'z'')$ from optical measurements even in the case of nominally smooth junctions.

In order to determine the form of $J_{\lambda\lambda'}(\mathbf{k}_p^{(0)},\omega \mid z'z'')$ theoretically, we must investigate the microscopic mech-

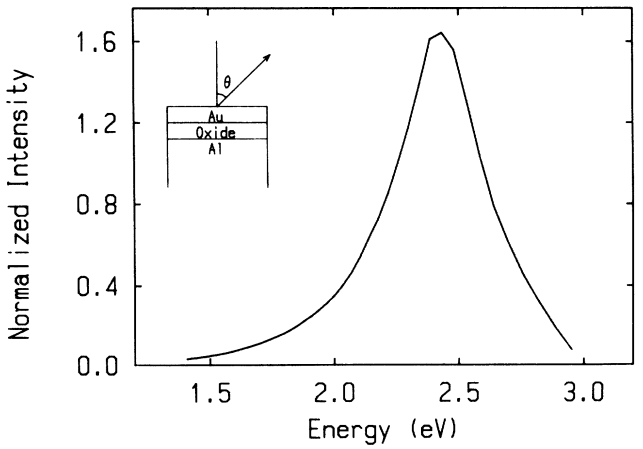

FIG. 17. All parameters are the same as in Fig. 16, except that the Al layer is made infinitely thick and the prism is removed.

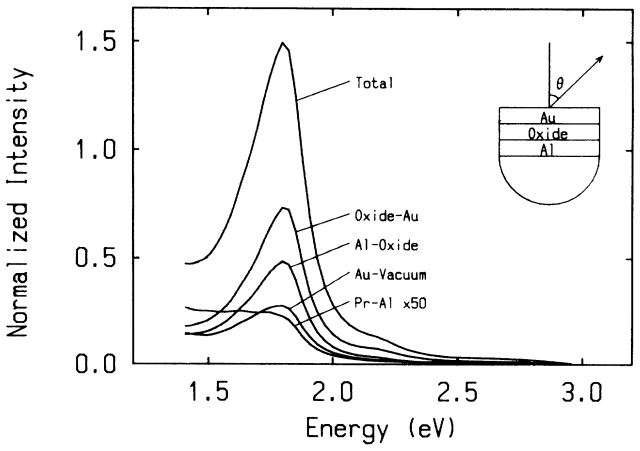

FIG. 19. *s*-polarized emission spectrum on the Au-vacuum side for the roughened prototype junction, showing separate contributions from different interfaces.

anisms of surface plasmon excitation by the tunneling current. This is a major theoretical task that has not yet been accomplished.

In the present theory as in paper III the effect of interface roughness was included by first-order perturbation on the Green's functions. A theory that includes higher-order perturbations representing multiple scattering of surface plasmons by roughness has been reported by Arya and Zeyher.[9] However, it is not clear at present whether multiple scattering by roughness is important as we see in the following experimental paper. It appears that determination of the precise form of $J_{\lambda\lambda'}(\mathbf{k}_p^{(0)},\omega \mid z'z'')$ is the more urgent task than the improvement of theory by inclusion of higher-order perturbation terms.

In a recent paper Pierce *et al.*[10] reported observation of light emission from the fast mode and the prism-Al mode. To fit the angle dependence of the emission by the two modes, they had to assume two current layers at the Au-air and Al-MgF_2 interfaces with the relative strength ratio of 3 to 1. Since the interface roughness acts as an effective current source, we believe that their result can be explained by assuming different amount of roughness at the two interfaces and one current fluctuation source across the oxide layer.

The mode conversion of the slow mode to the fast mode that is responsible for much of the emission has been experimentally observed by Gruhlke *et al.*[11] and Giergiel *et al.*[12] The theory reported by Giergiel *et al.* for mode conversion is essentially identical to the present one. The only difference is the source of excitation. In their case the surface plasmons are excited by an incident beam of a laser, while the source of excitation in the present case is the current fluctuation of the tunneling electrons.

V. CONCLUSION

By a comprehensive numerical study of the emission characteristics of light-emitting tunnel junctions, we have confirmed some of the earlier conjectures and discovered some new facts. Even in nominally smooth junctions, emission is dominated by the effect of roughness. In particular, the prism coupled *p*-polarized emission mainly arises from the fast mode that is generated by the scattering of the slow mode by interface roughness. This emission has the angle dependence characteristic of emission from the fast mode, but the population distribution of the fast mode is determined by the scattering of the slow mode into the fast mode. All other emissions (the *s*-polarized emission from both sides and the *p*-polarized emission from the Au-vacuum side) are caused by direct scattering of the slow mode into free external photons. The roughness at the oxide interfaces contributes most strongly to the emission process, indicating the importance of the slow mode as anticipated.

ACKNOWLEDGMENTS

We would like to acknowledge many valuable discussions with J. E. Rutledge, P. D. Sparks, D. L. Mills, R. M. Pierce, and J. Giergiel. This work was helped by financial assistances from the Japan-U.S. Scientific Cooperation Program of the Japan Society for Promotion of Science and the U.S. National Science Foundation, Murata Science Foundation, and Toray Science Foundation.

[1]An up-to-date list of references is found in P. Dawson, D. G. Walmsley, H. A. Quinn, and A. J. L. Ferguson, Phys. Rev. B **30**, 3164 (1984).

[2]S. Ushioda, J. E. Rutledge, and R. M. Pierce, Phys. Rev. Lett. **54**, 224 (1985).

[3]S. Ushioda, J. E. Rutledge, and R. M. Pierce, Phys. Rev. B **34**, 6804 (1986).

[4]B. Laks and D. L. Mills, Phys. Rev. B **20**, 4962 (1979).

[5]K. Kurosawa, R. M. Pierce, and S. Ushioda, Phys. Rev. B **33**, 789 (1986).

[6]J. Watanabe, A. Takeuchi, Y. Uehara, and S. Ushioda, following paper, Phys. Rev. B **38**, 12 959 (1988).

[7]M. A. Ordal, L. L. Long, R. J. Bell, S. E. Bell, R. R. Bell, R. W. Alexander, Jr., and C. A. Wood, Appl. Opt. **22**, 1099 (1983).

[8]P. B. Johnson and R. W. Christy, Phys. Rev. B **12**, 4370 (1972).

[9]K. Arya and R. Zeyher, Phys. Rev. B **28**, 4080 (1983).

[10]R. M. Pierce, J. E. Rutledge, and S. Ushioda, Phys. Rev. B **36**, 1803 (1987).

[11]R. W. Gruhlke, W. R. Holland, and D. G. Hall, Phys. Rev. Lett. **56**, 2838 (1986).

[12]J. Giergiel, C. E. Reed, J. C. Hemminger, and S. Ushioda, Phys. Rev. B **36**, 3052 (1987).